Geomechanics and Engineering, *Vol. 35, No. 2 (2023) 149-163*
https://doi.org/10.12989/gae.2023.35.2.149

Stability assessment of unlined tunnels with semicircular arch and straight sides in anisotropic clay

Bibhash Kumar[1a] and Jagdish P. Sahoo*[2]

[1]*Department of Civil Engineering, National Institute of Technology Uttarakhand 246174, India*
[2]*Department of Civil Engineering, Indian Institute of Technology Kanpur 208016, India*

(*Received May 10, 2022, Revised August 16, 2023, Accepted August 23, 2023*)

Abstract. This paper presents stability evaluation of unlined tunnels with semi-circular arch and straight sides (SASS) driven in non-homogeneous and anisotropic undrained clay. Numerical analysis has been conducted based on lower bound finite element limit analysis with second order cone programming under plane strain condition. The solutions will be used for the assessment of stability of unlined semi-circular arch tunnels and tunnels in which semi-circular roof is supported over rectangular/square sections. The stability charts have been generated in terms of a non-dimensional factor considering linear variation in undrained anisotropic strength for normally consolidated and lightly over consolidated clay with depth, and constant undrained anisotropic strength for heavily over-consolidated clay across the depth. The effect of normalized surcharge pressure on ground surface, non-homogeneity and anisotropy of clay, tunnel cover to width ratio and height to width ratio of tunnel on the stability factor and associated zone of shear failure at yielding have been examined and discussed. The geometry of tunnel in terms of shape and size, and non-homogeneity and anisotropy in undrained strength of clay has been observed to influence significantly the stability of unlined SASS tunnels.

Keywords: anisotropy; clay; non-homogeneous; stability; unlined tunnels

1. Introduction

During the process of underground excavation, the surrounding soil mass starts deforming which results in instability of underground openings as well as the structures residing on the ground surface. The movement of soil around the opening is driven by overburden soil pressure and surcharge at the ground surface, while this movement is restricted by shear strength of the soil mass. The stability of unlined tunnels is dependent on the combined interaction among the soil shear strength, loading conditions such as surcharge pressure and self-weight of soil mass, tunnel configurations like diameter/width and cover depth. Numerous investigations have been performed to study the stability of unlined tunnels in different types of soil. Davis *et al.* (1980) developed theoretical solutions for the stability evaluation of circular tunnel based on upper and lower bound theorem of plastic analysis. Using kinematic limit analysis, non-dimensional stability charts as well as deformation pattern for single tunnels (Osman *et al.* 2006) and unlined dual circular tunnels (Osman 2010) driven in undrained clay have been developed. Sahoo and Kumar (2012) and Sahoo and Kumar (2013a) generated the stability charts for single and dual circular tunnels constructed in cohesive-frictional soil employing upper bound finite element limit analysis.

Sahoo and Kumar (2013b) have conducted upper bound limit analysis for examining the stability of circular tunnels driven in undrained clay, where shear strength varies linearly with depth. The stability analysis of single unlined circular tunnel (Yamamoto *et al.* 2011), and dual unlined circular tunnel (Yamamoto *et al.* 2013) driven in cohesive-frictional soil subjected to surcharge loading have been performed using finite element concept of lower bound and upper bound limit analysis. From the aforementioned literature, it has been observed that circular tunnels have been employed most frequently despite the fact that their left, right, bottom and top spaces are mostly useless. This may be because (i) it is simple to construct circular tunnels from excavation and heading maintenance perspective; and (ii) circular tunnel yields high magnitude of stability number with-respect-to other geometries due to arching effect. However, trains and buildings are typically used underground, therefore noncircular apertures tunnels should be preferred in the design to maximize the use of the available area. Furthermore, the advancement of sophisticated tunneling machinery has led to the rapid emergence of large-size noncircular tunnels as a common building method. The noncircular cross-section of an underground opening has several advantages over circular ones, including smaller excavation sections, less surplus soil, which means fewer environmental concerns, and smaller rented sites for tunnel construction. Therefore, to effectively utilize the underground space, the current study assumes a non-circular opening having shape of the tunnel as semi-circular arch with straight sides (SASS); where, lower part is square or rectangular in shape and upper part (roof) is semi-circular arch. A very few studies (Wilson *et*

*Corresponding author, Ph.D.
E-mail: jpsahoo@iitk.ac.in
[a]Ph.D.
E-mail: bibhash.92@rediffmail.com a

ISSN: 2005-307X (Print), 2092-6219 (Online)

al. 2014, Zhang *et al.* 2018, Sun *et al.* 2021) has been found to be available in the literature for stability evaluation of tunnels with similar geometry as undertaken in the current study, assuming the soil mass to be homogeneous and isotropic. The shape of the tunnels is defined as horseshoe in these studies, which is completely different from the real geometry of horseshoe tunnels. Performing upper bound and lower bound plastic analysis, Wilson *et al.* (2014) have observed that the requirement of support pressure for SASS tunnel is less than that required for square/rectangular tunnel for the same span length. For stability analysis of dual SASS tunnel in cohesive-frictional soil mass, Zhang *et al.* (2018) have developed stability charts by executing upper bound analysis on the basis of FE formulation and adaptive meshing techniques. The failure mechanism and stability charts for dual unlined SASS tunnels advanced in isotropic non-homogeneous clay have been developed by Sun *et al.* (2021) by carrying out lower bound limit analysis.

All the above stability analyses assume the soil mass to be isotropic homogeneous/heterogeneous following either Tresca or Mohr-Coulomb yield criterion. In general, natural soil deposits of undrained clay exhibit some amount of anisotropy in term of shear strength owing to their loading, sedimentation and deposition process. The strength anisotropy is caused by stress induced anisotropy develops due to plastic deformation and loading of soil mass and inherent anisotropy develops due to initial fabric of soil mass during deposition (Casagrande and Carrillo 1944, Hansen and Gibson 1949, Lo 1965, Duncan 1966, Bishop 1966, Davis and Christian 1971, Lee and Rowe 1989, Ladd 1991). Ladd (1991) has discovered that strength anisotropy of undrained clay mainly depends upon the inclination of major principal stress (compressive in nature) with depositional direction or vertical axis, which is also conventionally adopted. Moreover, due to continuous increase in effective consolidation pressure with depth, natural deposits of undrained clay are non-homogeneous and showing a linear increment in the magnitude of undrained strength with depth in addition to strength anisotropy (Bishop 1966). The influence of strength non-homogeneity and anisotropy must be considered for developing more reliable solutions and accurate prediction of tunnel stability. A few studies (Lee and Rowe 1989, Pan and Dias 2015, Du *et al.* 2018, Haung *et al.* 2018, Ukritchon and Keawsawasvong 2018, 2020, Kumar and Sahoo 2021, 2023a,b,c, Sahoo and Kumar 2021) have been reported in the literature presenting the undrained stability charts for tunnels where anisotropy and non-homogeneity in shear strength was considered in the analysis. By establishing an elasto-plastic stress-strain soil model, Lee and Rowe (1989) were able to estimate the impact of anisotropic strength on the deformation behaviour of unlined and lined shallow tunnels in undrained clay. In order to evaluate the face stability of a tunnel advanced in an anisotropic and heterogeneous soil mass, Pan and Dias (2015) used a kinematic technique of limit analysis based-on 3D failure mechanism. Based on UBLA, Du *et al.* (2018) evaluated the impact of soil anisotropy and heterogeneity on the failure mechanism of the soil around the tunnel's periphery and earth pressure on the tunnel's sidewalls. Huang *et al.* (2018) have found solutions for the face stability of a circular tunnel advanced in anisotropic and heterogeneous soil using the 3D kinematic approach of limit analysis. The stability of square tunnels in undrained anisotropic homogeneous clay (Ukritchon and Keawsawasvong 2018) and in undrained anisotropic heterogeneous clay (Ukritchon and Keawsawasvong, 2020) has been analysed using lower bound limit analysis and non-dimensional charts were produced. Following the similar method of analysis as adopted in present study, non-dimensional stability charts have been generated for lined circular tunnel (Sahoo and Kumar 2021) and horseshoe-shaped tunnel (Kumar and Sahoo 2023a) in single layer anisotropic clay assuming linear variation of undrained strength with depth and for lined circular tunnel (Kumar and Sahoo 2023b) in two layered anisotropic undrained clay assuming strength to be constant within each layer.

Similarly, stability analysis of unsupported tunnels driven in anisotropic and non-homogeneous ground condition has been performed to develop the stability charts assuming the shape of the tunnel as circular (Kumar and Sahoo 2021) and horseshoe-shaped (Kumar and Sahoo 2023c). In addition, anisotropic behaviour in soil mass has been advocated for analysing many problems in geomechanics including stability analysis of slope (Xu *et al.* 2018), cavity expansion (Li and Zou 2019, Li *et al.* 2019, Cao *et al.* 2022) and embankment behaviour (Zhang *et al.* 2017).

So far, it seems that there is no universally acknowledged design or analysis method available that considers non-homogeneity and anisotropy in undrained shear strength of soil to evaluate the optimal magnitude of overburden pressure for maintaining stability analysis of unsupported SASS tunnels. Therefore, an effort has been made in this paper to analyse the stability of unlined SASS tunnels driven in nonhomogeneous anisotropic normally or lightly overconsolidated (NC/LOC) clay, and anisotropic heavily overconsolidated (HOC) clay following Davis and Christian (1971) yield criterion. The non-homogeneity in NC/LOC clay is incorporated by assigning an increment rate (m) at which undrained strength varies across the depth (Bishop, 1966); whereas anisotropy in NC/LOC and HOC clay are included by changing their strength relative to the inclination of major principal stress with the vertical direction. Two bound theorems of classical plasticity i.e., lower bound (LB) and upper bound (UB) are widely used with and without incorporation of finite elements and various optimization techniques for analysing the stability of tunnels taking into account complicated geometry of the problem, and complex loading and material conditions (Davis *et al.* 1980, Osman *et al.* 2006, Sahoo and Kumar 2012, Khezri *et al.* 2016, Yu 2018, Chen *et al.* 2019, Sahoo and Kumar 2019a,b, Kumar and Sahoo 2020a,b, Guo *et al.* 2021). In the lower bound analysis, the collapse load is computed from a statically admissible stress field that is the stress field which satisfy the equilibrium and boundary conditions without violating yield criterion anywhere in the chosen problem domain.

This collapse load would be either less or at the most

equal to true collapse load representing a pessimistic (or "safe") determination of collapse load. Whereas, in the upper bound analysis, the collapse load is determined by equating the rate of total work done by external and body forces to the rate of dissipation of total internal power in a kinematically admissible velocity field which satisfy velocity boundary conditions and velocity-strain compatibility conditions. The load computed from upper bound limit analysis remains always either higher or at the most equal to the true collapse load representing on the optimistic side of collapse load calculation. To obtain the solutions on the safer side, the lower bound limit analysis in conjunction with finite element formulation and second order conic programming has been utilized for performing the required numerical investigations in this study. The solutions were expressed in the form of non-dimensional charts, as a function of tunnel cover to width ratio (C/B) and height to width ratio (D/B) of the tunnel, linear strength increment ratio (m) with depth, anisotropic strength parameters (λ and μ) and surcharge pressure (σ_s) at the ground surface. Moreover, the zone of shear failure corresponding to the stress state at failure has also been developed for some specific cases.

2. Problem definition

This paper performs stability analysis of unlined semi-circular arch with straight sides (SASS) tunnels driven in saturated NC/LOC and HOC clay, subjected to uniformly distributed surcharge pressure on the ground surface. Fig. 1(a) illustrates the cross-sectional dimensions of SASS tunnel, where $B/2$ refers to the radius of semi-circular roof, and D and B represent height and width of tunnel, respectively. In order to perform plane strain analysis for the present problem, the length of the tunnel is assumed to be sufficiently large corresponding to its cross-sectional dimension. Depending upon the relation between B and D, the cross-sectional geometry of SASS tunnel becomes a square section at lower part with semi-circular roof for $D = 1.5B$, rectangular section at lower part with semi-circular roof for $D = B$, and semi-circular arch for $D = 0.5B$. The tunnel crown lies at a cover depth C below the ground surface. The anisotropic clay is fully saturated (angle of friction, $\phi_u = 0$) and assumed to behave like a perfectly plastic material following Davis and Christian failure criterion (Davis and Christian 1971) with an associated flow rule. The anisotropic behaviour of clay is characterized by three undrained strengths namely s_{u0}, s_{u45} and s_{u90} corresponding to the orientation of major principal stress measured from the vertical axis (ψ) equals to 0°, 45° and 90°, respectively, as presented in Fig. 1(b). The three undrained strengths s_{u0}, s_{u45} and s_{u90} can be described in term of dimensionless parameters by introducing two anisotropic strength coefficients λ and μ, which can be defined as, $\lambda = s_{u90}/s_{u0}$ and $\mu = s_{u45}/s_{u0}$. In the current study, the soil can be characterized as isotropic or anisotropic NC/LOC undrained clay and HOC undrained clay, depending upon the magnitude of λ and μ as suggested by Lee and Rowe (1989). The soil behaves like (i) isotropic undrained clay, when $\lambda = \mu = 1$; (ii) anisotropic NC/HOC clay, when $\lambda \leq 1$ and $\lambda < \mu < 1$; and (iii) anisotropic HOC clay, when $\lambda \geq 1$ and $\mu \leq \lambda$. The anisotropic NC/LOC clay is considered non-homogeneous whose undrained strength varies almost linearly with depth, while the HOC clay is assumed to be homogeneous i.e. undrained strength remains unchanged throughout the depth. The variation in the value of anisotropic undrained strength of NC/LOC clay with depth d below the horizontal ground surface can be expressed as

$$s_{u0} = s_{u0s}\left(1 + m\frac{d}{B}\right) \tag{1a}$$

$$s_{u45} = s_{u45s}\left(1 + m\frac{d}{B}\right) \tag{1b}$$

$$s_{u90} = s_{u90s}\left(1 + m\frac{d}{B}\right) \tag{1c}$$

where, m refers to the rate of increment of undrained strength with depth. For ψ = 0°, 45° and 90°, (i) s_{u0s}, s_{u45s} and s_{u90s} signify shear strength at ground surface, respectively, and (ii) s_{u0}, s_{u45} and s_{u90} refer to shear strength at any depth d below ground surface, respectively. It needs to be noted that the magnitude of μ and λ remains unchanged across the depth. The stability of unlined SASS tunnel can be expressed in term of non-dimensional stability factor as

$$N_s = \gamma C / s_{u0s} \tag{2}$$

where, γ represent weight per unit volume (unit weight) of undrained clay that can be withstand by unsupported SASS tunnel without any collapse due to surrounding soil mass for a particular combination of depth (D) and width (B) of tunnel, total cover-depth (C), linear strength increment ratio (m), anisotropic strength parameters (λ and μ) or undrained strengths (s_{u0}, s_{u45}, s_{u90}) and surcharge pressure (σ_s) at the ground surface. For different combinations of σ_s/s_{u0s}, m, λ, μ, C/B and H/B, it is intended to compute the optimum value of γ in the present analysis.

3. Analysis

In this study, the concept of finite element lower bound limit analysis (Sloan, 1988), which combines the techniques of finite element discretization and lower bound theorem of plasticity, and second order cone programming techniques of mathematical optimization (Makrodimopoulos and Martin 2006) have been adopted to investigate the undrained stability of unlined SASS tunnels in non-homogeneous and anisotropic clay. The surcharge pressure (σ_s) on the ground surface and self-weight of undrained clay (γ) are the external and body forces, respectively cause instability of soil surrounding the tunnels leading to failure. Therefore, the magnitude of self-weight of undrained clay for different value of surcharge pressure has been maximized by satisfying the following requirements: (i) element equilibrium conditions; (ii) stress boundary conditions; (iii) continuity of shear and normal stresses along stress discontinuities; and (iv) non-violation of yield criterion. For preparing model of the present problem, a

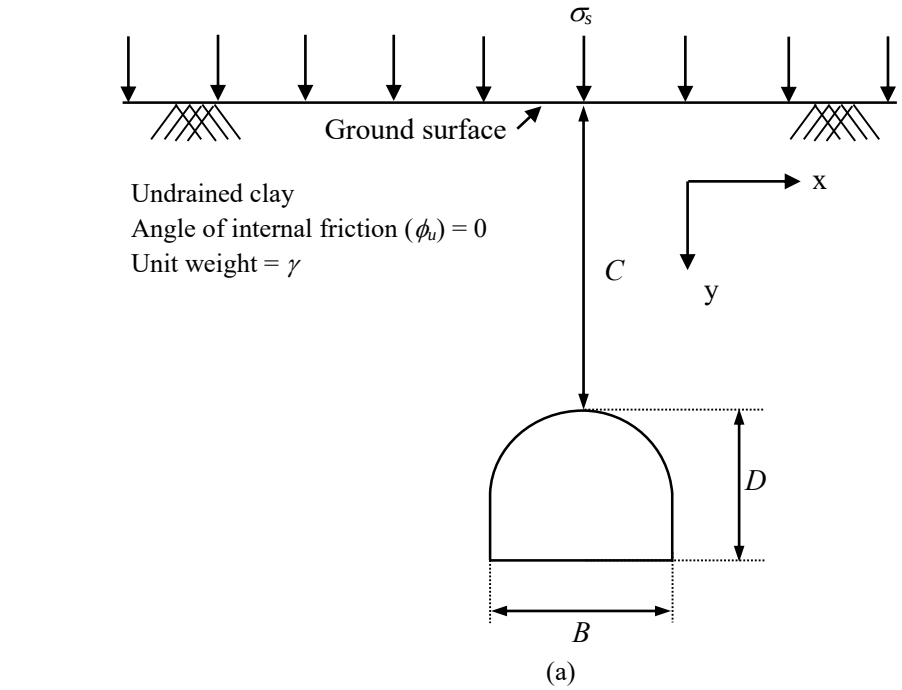

(a)

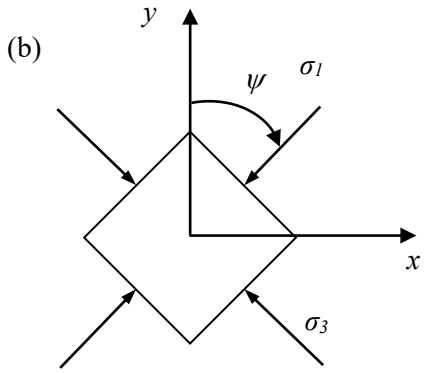

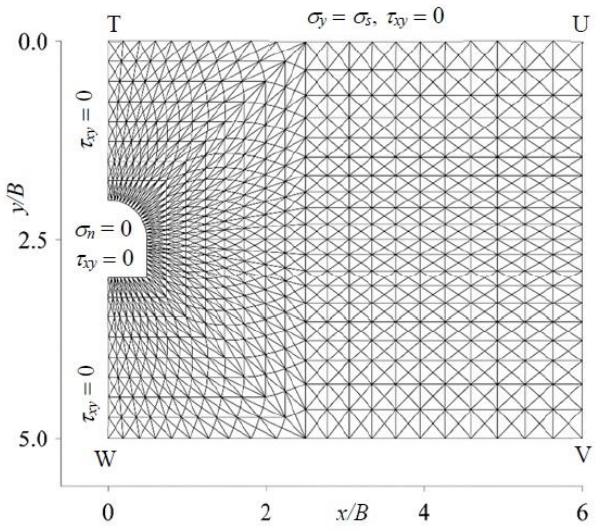

(b) (c)

Fig. 1 (a) Definition of problem, (b) inclination of major principal stress with vertical for defining anisotropic strength variation; and (c) a typical finite element mesh for *C/B* = 2 along with associated boundary conditions

symmetrical condition from geometry and loading standpoint at the centreline of the problem domain has been utilized. As a consequence, only half of the chosen domain is considered for carrying out the present stability analysis. Necessary programming codes have been written in MATLAB for discretization of undrained clay using three noded linear triangular elements. The chosen problem domain TUVW along with a typical finite element mesh for *C/B* = 2 is illustrated in Fig. 1(c). Each node of the triangular elements has three unknown nodal stresses (σ_{xx}, σ_{yy} and τ_{xy}) under 2D Cartesian stress states. The variation of unknown stress components within each triangular element is in compliance with the static element equilibrium conditions as follows

$$\frac{\partial \sigma_{xx}}{\partial x} + \frac{\partial \tau_{xy}}{\partial y} = 0 \tag{3a}$$

$$\frac{\partial \sigma_{yy}}{\partial y} + \frac{\partial \tau_{xy}}{\partial x} = \gamma \tag{3b}$$

where, γ is the weight per unit volume (unit weight) of undrained clay.

It may be noted that incorporation of stress discontinuities in lower bound analysis is essential to achieve the numerical results closer to exact solutions (Drucker 1953) and can be obtained by allowing the value of shear and normal stresses continuous along the shared

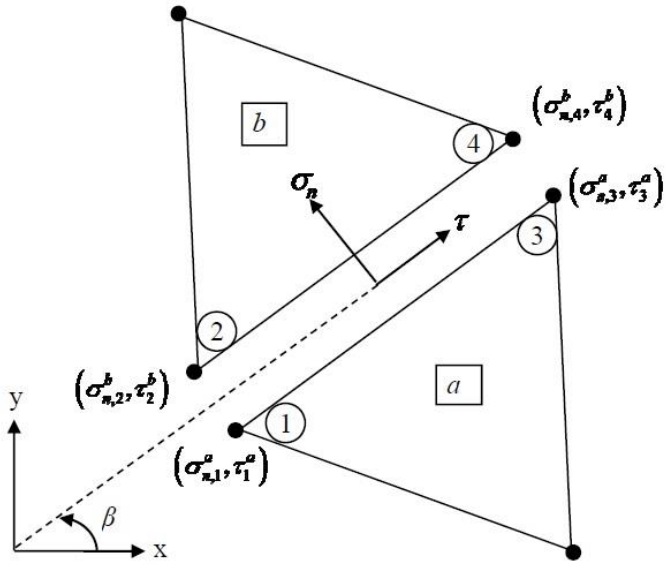

Fig. 2 Statically admissible stress discontinuity between two adjacent elements

plane of adjacent elements (Sloan 1988). To attain this, in the present analysis, nodes assigned to triangular elements are unique for a specific element so that various nodes share single coordinates and hence the conditions of stress discontinuities are satisfied along a shared plane of the adjacent triangular element. From Fig. 2, it may be noted that nodes 1 and 2 have same coordinate but they are unique to the respective elements "a" and "b". The stress field at node 1 (σ_{x1}, σ_{y1} and τ_{xy1}) and 2 (σ_{x2}, σ_{y2} and τ_{xy2}) are different and lead to the formation of stress discontinuity along the shared edge of elements "a" and "b". Thus, to maintain the equilibrium conditions of the stress field along the stress discontinuity (i.e., along shared edge of the two elements a and b), it is necessary to enforce additional constraints as

$$\sigma^a_{n,1} = \sigma^b_{n,2};\ \tau^a_1 = \tau^b_2;\ \sigma^a_{n,3} = \sigma^b_{n,4};\ \tau^a_3 = \tau^b_4 \tag{4}$$

where,

$$\sigma^a_{n,1} = \sin^2\beta\sigma^a_{x1} + \cos^2\beta\sigma^a_{y1} - \sin 2\beta\tau^a_{xy1}$$

$$\tau^a_1 = -\frac{1}{2}\sin 2\beta\sigma^a_{x1} + \frac{1}{2}\sin 2\beta\sigma^a_{y1} + \cos 2\beta\tau^a_{xy1}$$

$$\sigma^b_{n,2} = \sin^2\beta\sigma^b_{x2} + \cos^2\beta\sigma^b_{y2} - \sin 2\beta\tau^b_{xy2}$$

$$\tau^b_2 = -\frac{1}{2}\sin 2\beta\sigma^b_{x2} + \frac{1}{2}\sin 2\beta\sigma^b_{y2} + \cos 2\beta\tau^b_{xy2}$$

Similarly, the expressions for $\sigma^a_{n,3}$, τ^a_3, $\sigma^b_{n,4}$ and τ^b_4 can be written.

The dimension of bottom horizontal boundary (WV) and right vertical boundary (UV) of the chosen domain are kept large enough, such that the failure zone does not intersect the boundaries and remain contained well within the chosen domain; moreover, the value of stability factor does not alter with further increase in the domain size. Fig. 1(c) provides the details of stress boundary conditions as: (i) along the periphery of unlined tunnel, $\sigma_n = \tau = 0$; (ii) along the ground surface (TU), $\sigma_n = \sigma_s$ and $\tau = 0$; (iii) along the left centre line boundary (TW), $\tau = 0$ and σ_n = unconstrained; and (iv) along rest boundaries (UV and WV), $\sigma_n = \tau$ = unconstrained.

In lower bound theorem, the stress state must not violate the yield function at each triangular node within the problem domain. For ensuring the state of stress lies within the triangular element, Davis and Christian strength criterion (Davis and Christian 1971) can be written as

$$\left[\left(\frac{\sigma_{yy} - \sigma_{xx}}{2} - \frac{s_{u0} - s_{u90}}{2}\right)^2 + \tau^2_{xy}\left(\frac{s_{u0}s_{u90}}{s^2_{u45}}\right)\right]^{1/2} \le \left(\frac{s_{u0} + s_{u90}}{2}\right) \tag{5}$$

The above anisotropic yield function (Eq. (5)) can be represented as a set of second order constraints by following the techniques of second order cone programming (Makrodimopoulos and Martin 2006) as

$$Z^2_2 + Z^2_3 \le Z^2_1 \tag{6}$$

where, z_1, z_2 and z_3 are auxiliary stress variables and defined as

$$z_1 = \frac{s_{u0} + s_{u90}}{2} \tag{7a}$$

$$z_2 = \frac{\sigma_{yy} - \sigma_{xx}}{2} - \frac{s_{u0} - s_{u90}}{2} \tag{7b}$$

$$z_3 = \tau_{xy}\frac{\sqrt{s_{u0}s_{u90}}}{s_{u45}} \tag{7c}$$

Eq. (5) can be transformed into equality constraints matrix as follows

$$A_{soc}\sigma + z = b_{soc} \tag{8}$$

$$A_{soc}=\begin{bmatrix} 0 & 0 & 0 \\ \frac{1}{2} & -\frac{1}{2} & 0 \\ 0 & 0 & -\frac{\sqrt{s_{u0}s_{u90}}}{s_{u45}} \end{bmatrix};$$

$$\sigma=\begin{bmatrix}\sigma_{xx}\\ \sigma_{yy}\\ \tau_{xy}\end{bmatrix};\ z=\begin{bmatrix}z_1\\ z_2\\ z_3\end{bmatrix};\ b_{soc}=\begin{bmatrix}\frac{s_{u0}+s_{u90}}{2}\\ -\frac{s_{u0}-s_{u90}}{2}\\ 0\end{bmatrix}$$

In order to conduct the lower bound stability analysis of unlined SASS tunnel, the objective function is maximized i.e. the self-weight of undrained clay is maximized subject to a number of statically admissibility stress conditions. The final form of second order cone programming can be expressed as:

$$\text{Objective function:} \quad \text{Maximize} \quad \gamma \tag{9a}$$

$$\text{Constraints:} \quad [A]\{\sigma\}+[T]\{z\}=\{B\} \tag{9b}$$

where, $\{z\}$ and $\{\sigma\}$ are the auxiliary stress variables and nodal stresses, $[A]$ and $\{B\}$ are the matrixes and vectors of all constraints for stress boundary conditions, stress discontinuities, element equilibrium conditions and yield criterion. $[T]$ is the matrix representing the relationship between auxiliary variables and nodal stresses. The standard form of second order cone programming as presented in Eq. (9) can be expressed in the following format to perform the optimization using MOSEK

$$\text{Maximize } \gamma \tag{10a}$$

$$B_l \le [A]\{u\} \le B_u \tag{10b}$$

$$b_l \le \{u\} \le b_u \tag{10c}$$

For obtaining optimal solutions of current optimization problem in Eq. (10), a conic optimizer toolbox MOSEK ApS. (2015) accessible for MATLAB (2015) has been adopted. For the primary problem expressed in Eq. (10), the *prob* data structure with several subfields is defined as:

prob.c = $\boldsymbol{\gamma}$ (defines the objective function)

prob.a = $\boldsymbol{A}$ (refers to constraints matrix)

prob.buc = $\boldsymbol{B_u}$ and *prob.blc* = $\boldsymbol{B_l}$ (represent the upper bound and lower bound for the constraints, respectively);

prob.bux = **[ ]** and *prob.blx* = **[ ]** are upper and lower bound for the variables, respectively.

Finally, the type of cone and the member variables of the cone has been specified as *prob.cones.type* and *prob.cones.sub* using the following code:

prob.cones = *cell* (*N*, 1);

for j = 1: *N*

prob.cones{j}.type = 'MSK_CT_QUAD';

prob.cones{j}.sub = [3**N*+1+3*j-2, 3**N*+1+3*j-1, 3**N*+1+3*j];

end

res = mosekopt ('maximize', prob);

where, *N* represents total number of nodes. Using "mosekopt" in MOSEK, the optimization of objective function can be done after solving the primal and dual programming simultaneously. The optimal value of collapse load is obtained by using the command "*res.sol.itr.pobjval*"

4. Verification of present numerical solutions

Fig. 3 illustrates the verification of present numerical formulation by comparing solutions obtained from the present analysis with those reported in the literature. The variation of stability factor (N_s) computed from the present analysis are compared with the solutions of (i) Wilson *et al.* (2014) as presented in Fig. 3(a) for SASS tunnels driven in homogeneous and isotropic undrained clay with *D/B* = *C/B* = 1; (ii) Kumar and Sahoo (2021) for circular tunnel and Ukritchon and Keawsawasvong (2020) for square tunnel constructed in homogeneous and anisotropic undrained clay as illustrated in Figs. 3(b) and 3(c), respectively.

The numerical analysis performed by Wilson *et al.* (2014), Kumar and Sahoo (2021) and Ukritchon and Keawsawasvong (2020) are on the basis of lower bound limit analysis coupled with finite element formulation and nonlinear optimization techniques. For verification purpose, a few computations have also been performed in the present analysis to compute stability factor (N_s) for unlined square tunnels in homogeneous and isotropic clay as illustrated in Fig. 3(c). It needs to mention that the magnitude of μ is being taken as $2\lambda/(1+\lambda)$ corresponding to a particular magnitude of λ as taken by Ukritchon and Keawsawasvong (2020), which is presented in Fig. 3(c). As expected, the present numerical solutions for SASS and square tunnels are exactly matching with results of Wilson *et al.* (2014) and Ukritchon and Keawsawasvong (2020). For the same height and width of SASS tunnel as compared to that of diameter/width of circular/square tunnel, it needs to mention that stability factor (N_s) for SASS tunnel is lower as compared to circular tunnel (Fig. 3(b)) and higher than that of square tunnel (Fig. 3(c)).

5. Results and discussions

The optimum values of γ computed from the present analysis have been presented as a dimensionless stability factor ($N_s = \gamma C/s_{uos}$) which is related to collective interaction between (i) height to width ratio (D/B) of tunnel, (ii) cover to width ratio (C/B) of tunnel, (iii) linear strength increment ratio (m), (iv) anisotropic strength parameters (λ and μ) and (v) surcharge pressure (σ_s) on the ground surface. The variation in the magnitude of anisotropic strength parameters λ (s_{u90}/s_{u0}) and μ (s_{u45}/s_{u0}) for NC/LOC clay is found to be 0.59-0.95 and 0.62-0.99, respectively, however, for HOC clay, the variation is noted to be 1.05-1.46 and 0.78-1.18, respectively (Jakobson 1955, Hvorslev 1960, Lo 1965, Bishop 1966, Duncan and Seed 1966, Lo and Milligan 1967, Saada 1972, Lee and Rowe 1989).

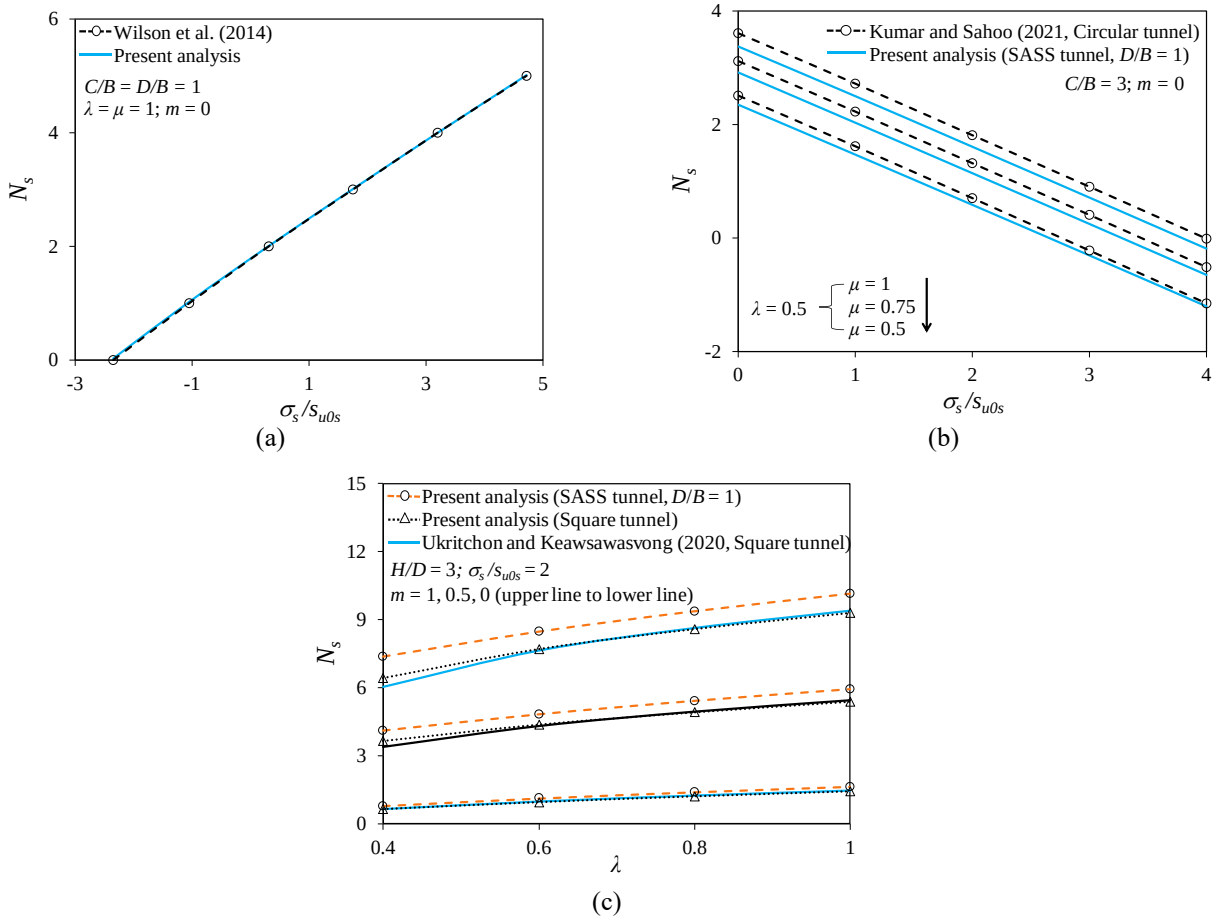

Fig. 3 Comparison of present solutions with that of (a) Wilson *et al.* (2014), (b) Kumar and Sahoo (2021); and (c) Ukritchon and Keawsawasvong (2020)

Table 1 A comparison of N_s between isotropic and anisotropic normally consolidated clay for different values of σ_s/s_{u0s}, C/B, D/B and m

m	σ_s/s_{u0s}	C/B	$\lambda = 0.5; \mu = 0.5$			$\lambda = 0.5; \mu = 1$			$\lambda = 1; \mu = 1$		
			$D/B = 0.5$	$D/B = 1$	$D/B = 1.5$	$D/B = 0.5$	$D/B = 1$	$D/B = 1.5$	$D/B = 0.5$	$D/B = 1$	$D/B = 1.5$
0	0	1	1.29	1.27	1.16	2.10	1.81	1.54	2.13	1.83	1.55
		3	2.65	2.35	2.12	3.90	3.37	2.98	4.07	3.41	3.00
		5	3.39	2.98	2.69	4.80	4.23	3.79	5.17	4.41	3.86
	2	1	-0.51	-0.52	-0.53	0.39	0.28	0.22	0.43	0.31	0.24
		3	0.77	0.58	0.47	2.03	1.61	1.32	2.18	1.64	1.34
		5	1.47	1.13	0.92	2.89	2.40	2.04	3.24	2.56	2.09
1	0	1	2.23	2.22	2.21	3.89	3.68	3.48	3.91	3.75	3.59
		3	8.45	8.43	8.40	12.74	11.81	11.14	13.11	11.93	11.15
		5	16.16	15.26	14.67	23.49	21.40	19.95	24.67	21.92	20.15
	2	1	0.40	0.39	0.38	2.12	2.06	2.00	2.15	2.10	2.07
		3	6.54	6.52	6.50	10.84	10.00	9.44	11.22	10.15	9.47
		5	14.22	13.39	12.87	21.55	19.52	18.14	22.74	20.06	18.36

For different combinations of σ_s/s_{u0s}, D/B, C/B, λ and μ, the numerical solutions for stability analysis of unlined SASS tunnel are computed as follows: (i) by varying the magnitude of anisotropic undrained strength with depth (m = 0, 0.5 and 1) in case of NC/LOC clay, and (ii) by keeping the magnitude of anisotropic undrained strength constant across the depth (m = 0) in case of HOC clay. It needs to be mentioned that the influence of λ on stability factor is observed to be insignificant from the Fig. 4, plotted for some typical cases

Therefore, the solutions for stability factors in the case of NC/LOC clay are obtained corresponding to λ = 0.5 with

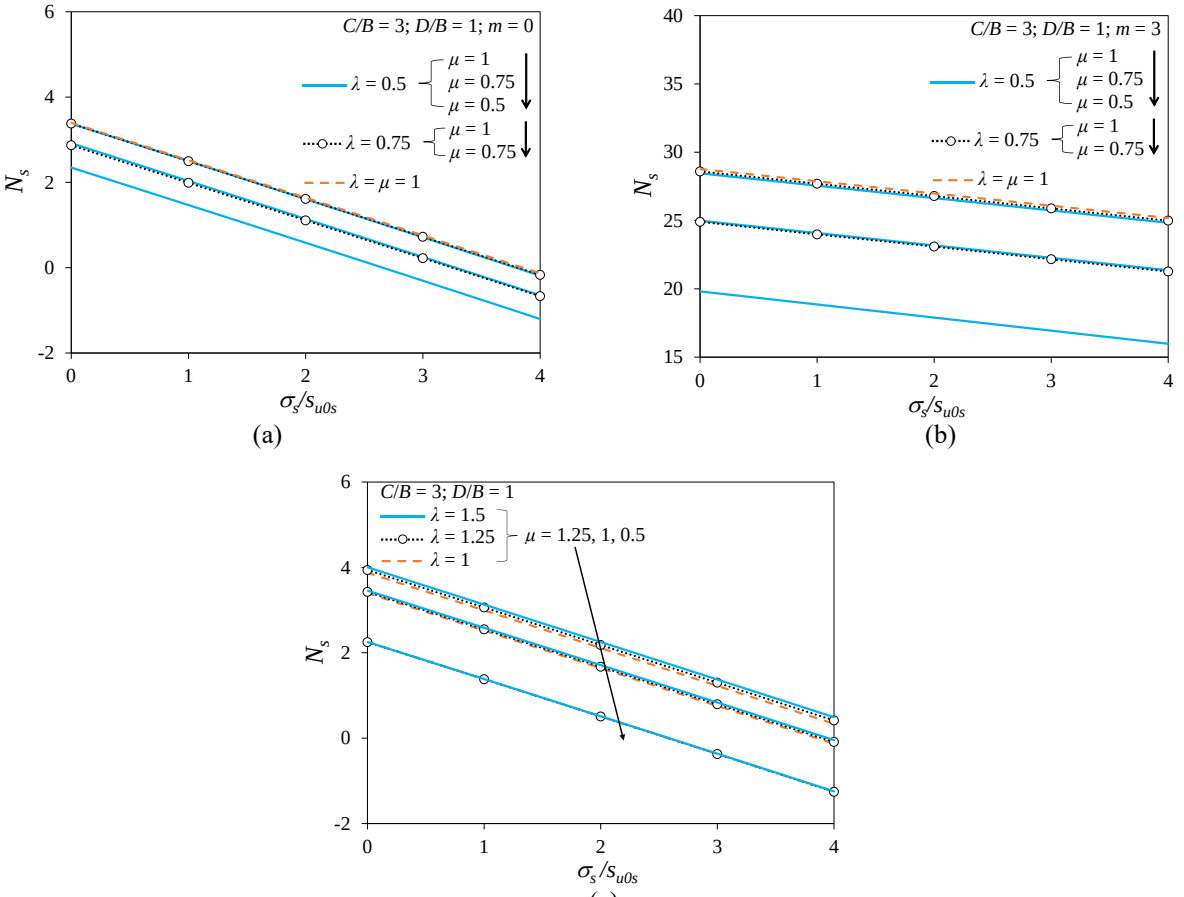

Fig. 4 For D/B = 1, variation of N_s with σ_s/s_{u0s} for different value of λ and μ in case of (a) NC/LOC clay with C/B = 3 and m = 0; (b) NC/LOC clay with C/B = 3 and m = 1; and (c) HOC clay with C/B = 3

Table 2 A comparison of N_s between isotropic and anisotropic heavily consolidated clay for different values of σ_s/s_{u0s}, C/B, D/B, and μ

σ_s/s_{u0s}	C/B	λ = 1.5; μ = 0.5			λ = 1; μ = 1			λ = 1.5; μ = 1.25		
		D/B = 0.5	D/B = 1	D/B = 1.5	D/B = 0.5	D/B = 1	D/B = 1.5	D/B = 0.5	D/B = 1	D/B = 1.5
0	1	1.20	1.18	1.11	2.13	1.83	1.55	2.46	2.05	1.72
	3	2.61	2.25	2.02	4.07	3.41	3.00	4.92	4.00	3.42
	5	3.46	2.88	2.57	5.17	4.41	3.86	6.34	5.26	4.54
2	1	-0.59	-0.61	-0.63	0.43	0.31	0.24	0.79	0.60	0.47
	3	0.74	0.51	0.40	2.18	1.64	1.34	3.04	2.25	1.79
	5	1.55	1.05	0.82	3.24	2.56	2.09	4.43	3.42	2.78

μ ranging from 0.5 to 1 as presented in Figs. 5-7; whereas, for HOC clay, the stability factors were computed corresponding to λ = 1.5 for μ varying from 0.5 to 1.25, as illustrated in Fig. 8. The stability factor (N_s) for D = 1.5B, B and 0.5B as presented in Figs. 5-8, corresponds to square section at lower part with semi-circular roof, rectangular section at lower part with semi-circular roof and semi-circular arch, respectively.

From Figs. 5-8, (i) the maximum depth of tunnel crown below the horizontal ground surface (C/B) for a given value of surcharge pressure (σ_s/s_{u0s}) on ground surface, and (ii) the maximum value of surcharge pressure (σ_s/s_{u0s}) on the ground surface for a certain value of tunnel cover depth (C/B), which can be allowed without any support system around tunnel periphery, will be determined for given geometries of SASS tunnel and soil properties.

As illustrated in Figs. 5-8, the stability factor represented with positive sign signifies that surrounding soil mass around tunnel periphery remains stable without any support systems, which further enhances with increase in the magnitude of stability factor. However, the stability factor with negative sign indicates that support system needs to be installed around tunnel periphery to maintain stability of surrounding soil mass. For different combinations of σ_s/s_{u0s}, C/B, m and μ, the magnitude of stability factor (N_s) is observed to be higher for tunnel with

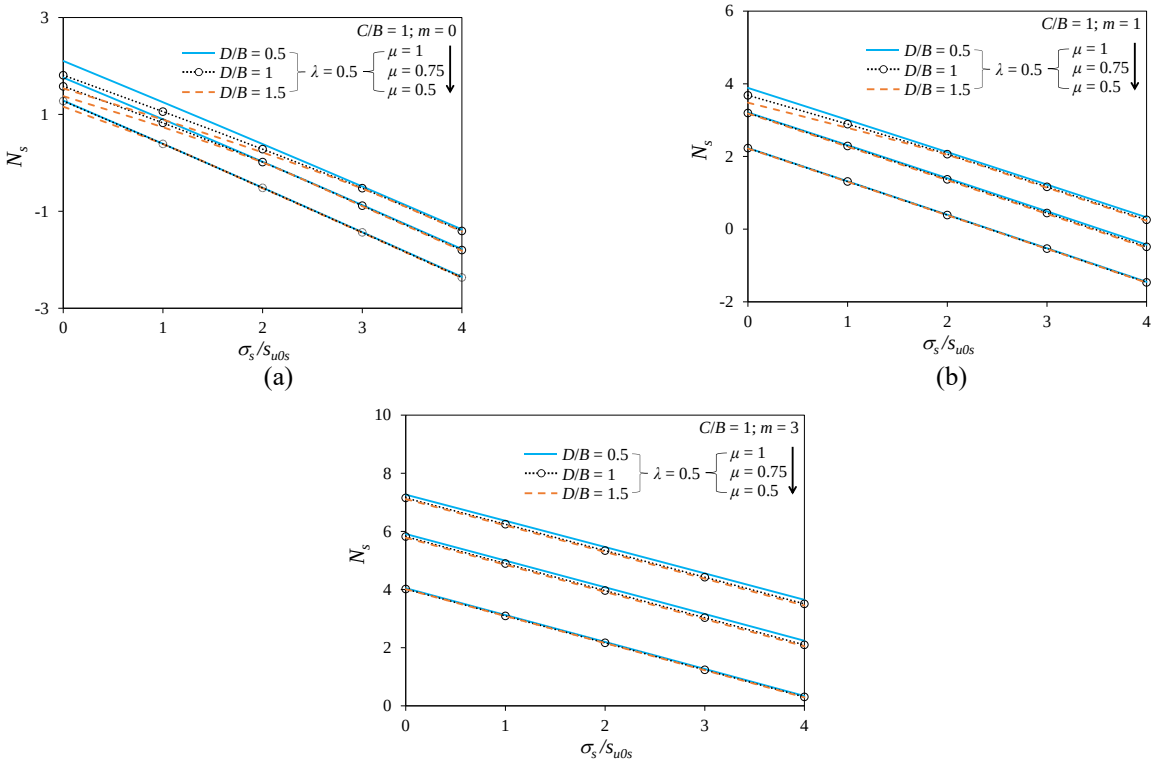

Fig. 5 For NC clay with C/B = 1, variation of N_s with σ_s/s_{u0s} for λ = 0.5 and different value of μ and D/B: (a) m = 0; (b) m = 1; and (c) m = 3.

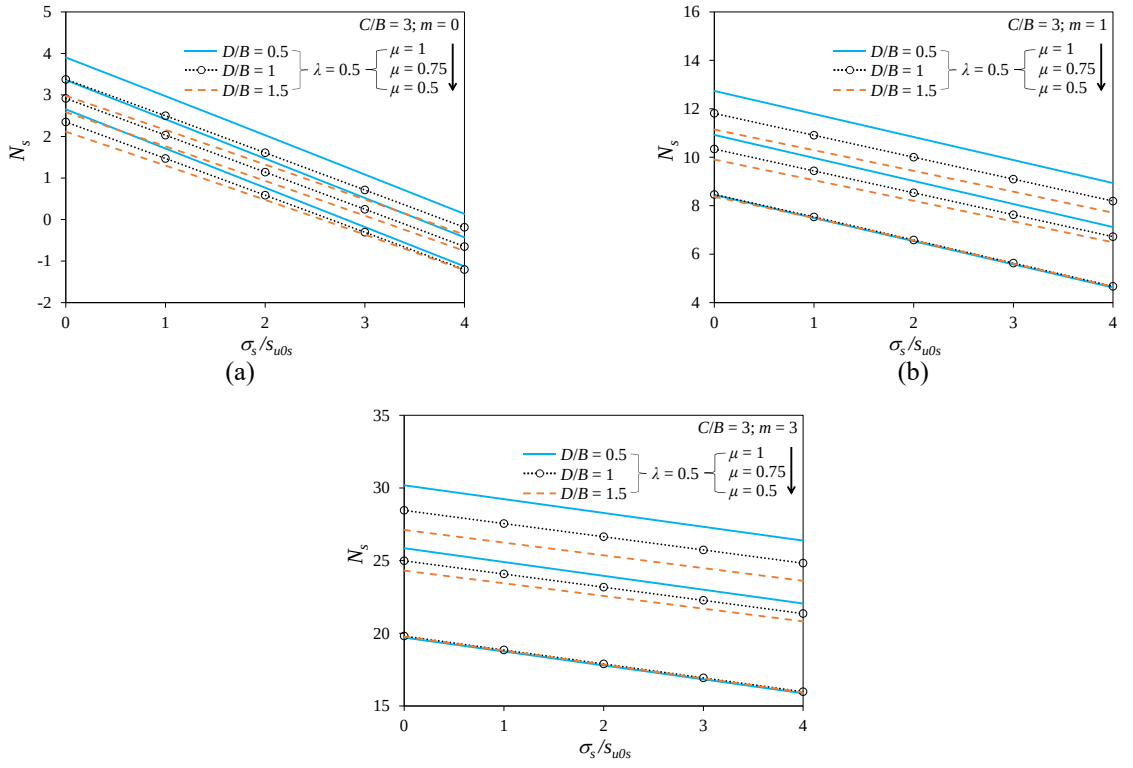

Fig. 6 For NC clay with C/B = 3, variation of N_s with σ_s/s_{u0s} for λ = 0.5 and different value of μ and D/B: (a) m = 0, (b) m = 1; and (c) m = 3

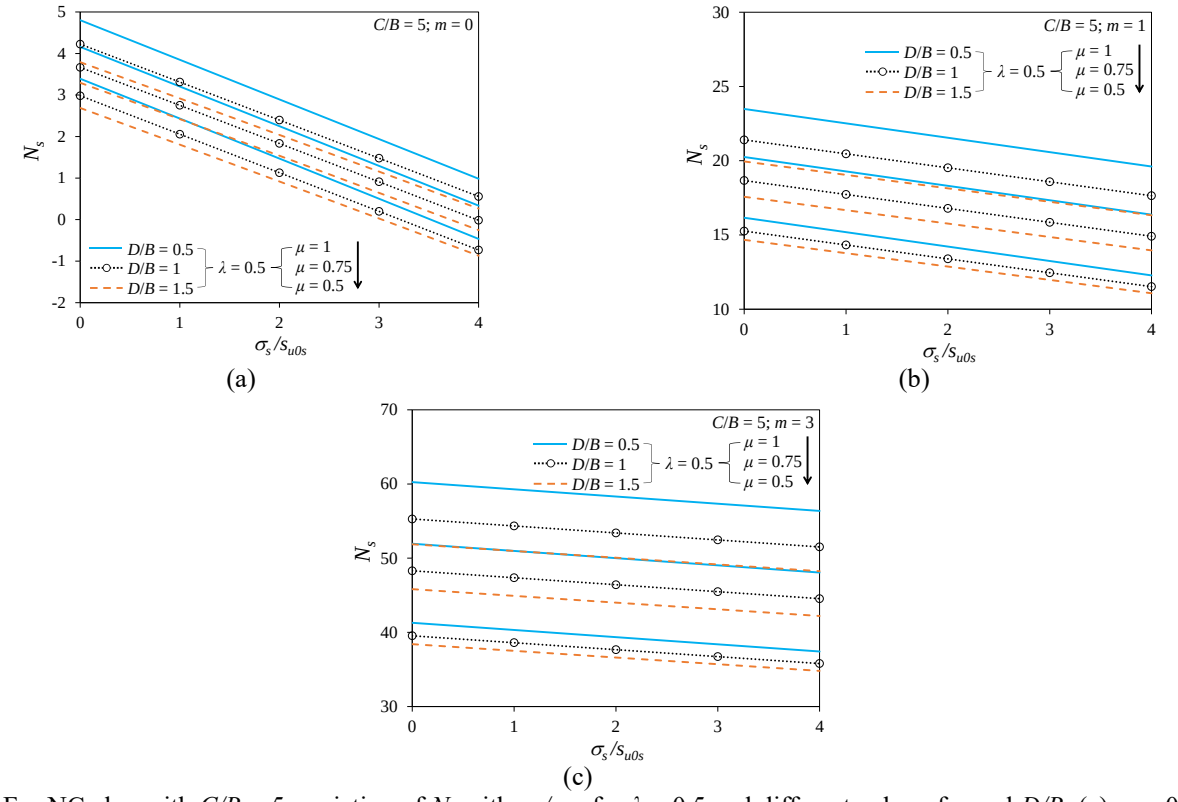

Fig. 7 For NC clay with C/B = 5, variation of N_s with σ_s/s_{u0s} for λ = 0.5 and different value of μ and D/B: (a) m = 0, (b) m = 1; and (c) m = 3

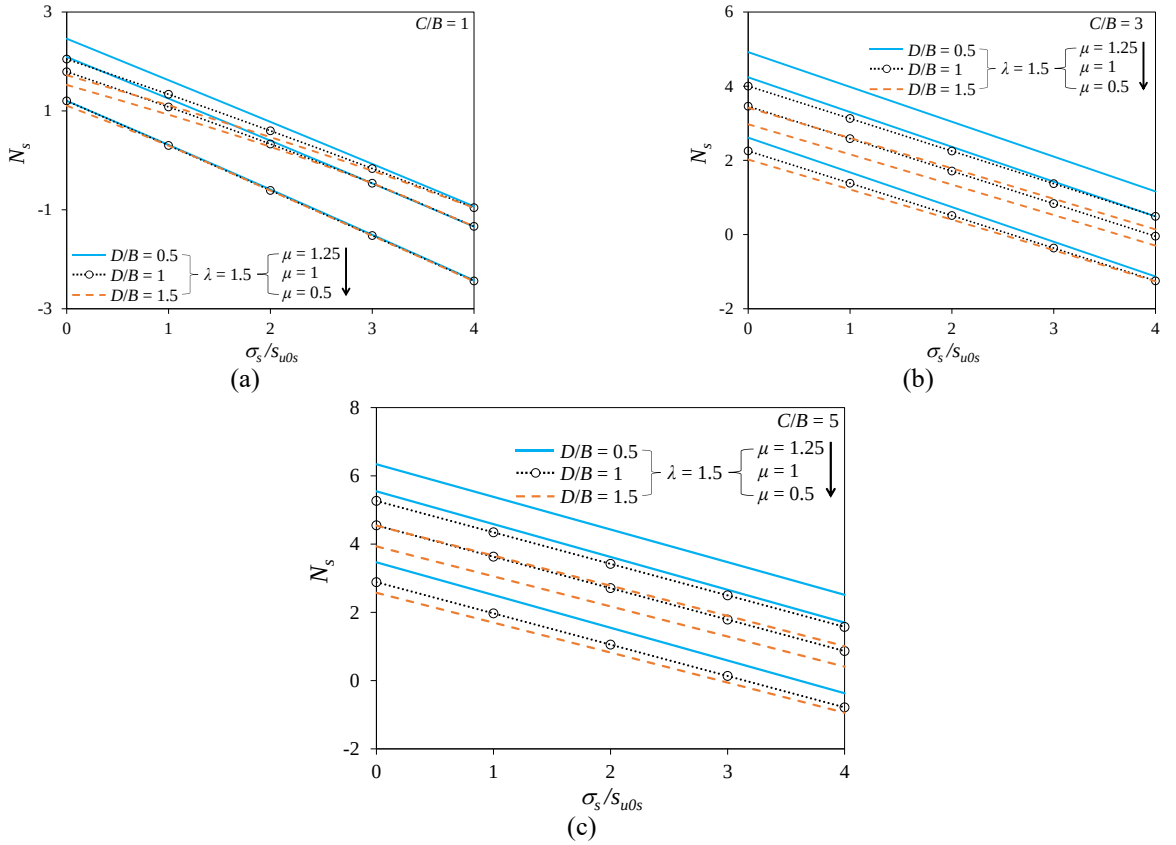

Fig. 8 For HOC clay, variation of N_s with σ_s/s_{u0s} for λ = 1.5 and different value of μ and D/B: (a) C/B = 1, (b) C/B = 3; and (c) C/B = 5

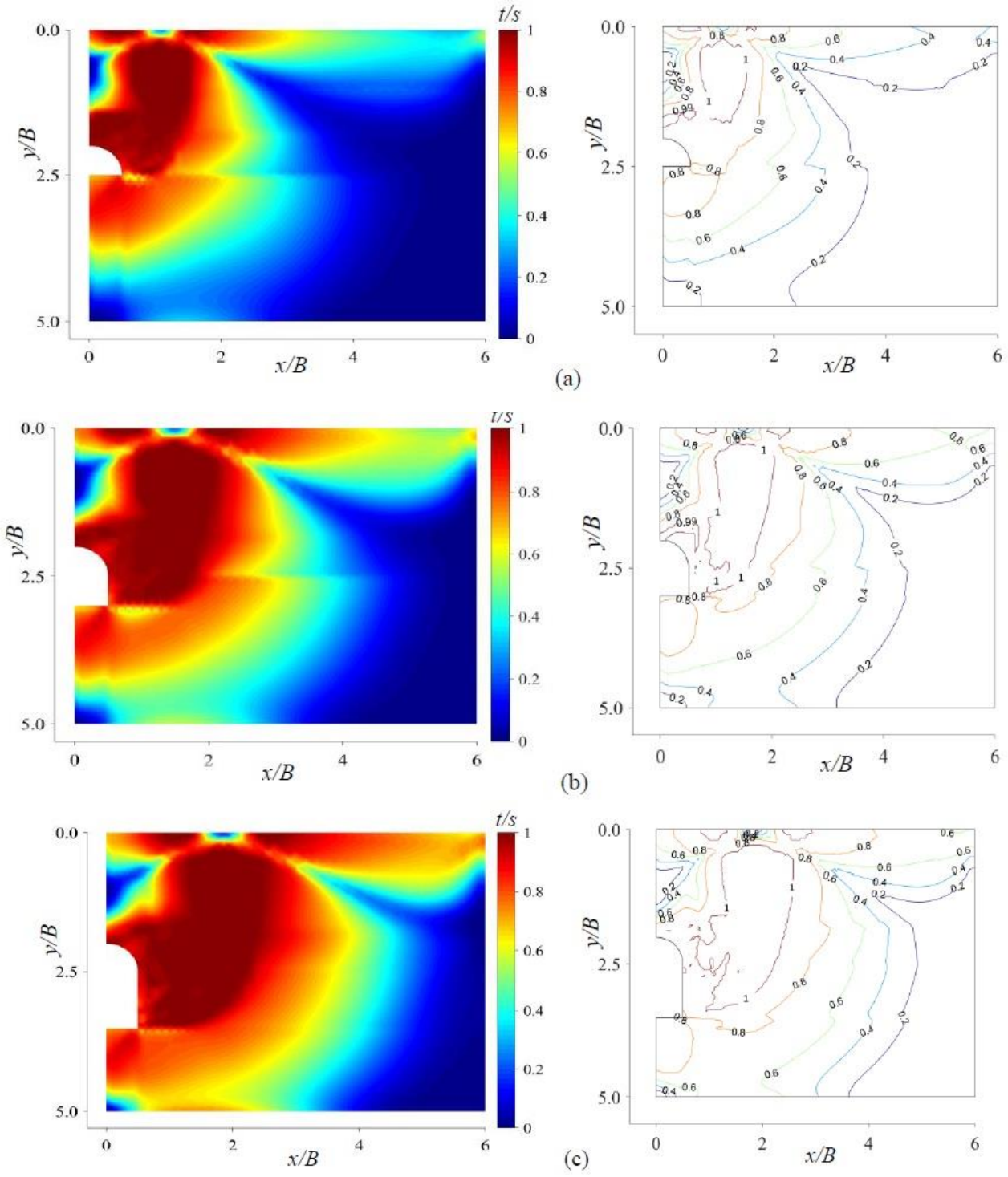

Fig. 9 Failure pattern and contour lines in NC/LOC clay for C/B = 2, σ_s/s_{u0s} = 0, λ = μ = 1 and m = 0: (a) D/B = 0.5, (b) D/B = 1 and (c) D/B = 1.5.

lower height to width ratio (D/B) and lowest for tunnel having square section at lower part with semi-circular roof. With continuous increase in the magnitude of C/B and decrease in the value of surcharge pressure (σ_s/s_{u0s}), the stability factor (N_s) is observed to be increasing. This implies that with increase in cover depth of tunnel and with reduction in the value of surcharge pressure, the stability of unlined SASS tunnel enhances.

Tables 1 and 2 present the magnitude of stability factor (N_s) for SASS tunnel constructed in NC/LOC and HOC clay for a few combinations of σ_s/s_{u0s}, C/B, D/B, m and μ. For different combinations of μ and D/B, the values of N_s for anisotropic clay have been observed to be always (i) lower in comparison to that computed for isotropic NC/LOC clay as observed from Table 1 and Figs. 5-7; and (ii) lower/higher than that computed for isotropic HOC clay

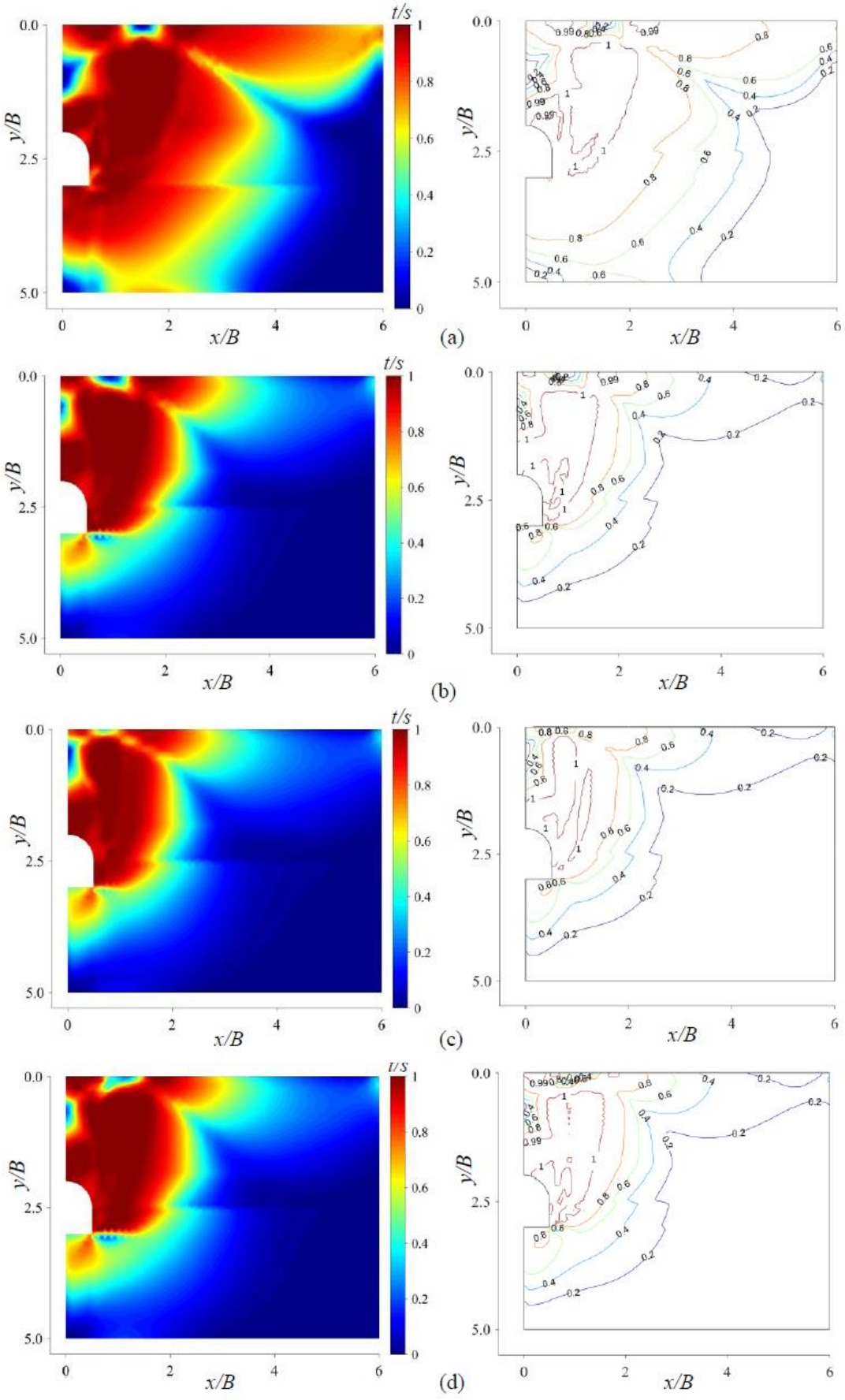

Fig. 10 Failure pattern and contour lines in NC/LOC clay for $C/B = 2$, $D/B = 1$ and $\lambda = 0.5$: (a) $\mu = 0.5$, $m = 0$, $\sigma_s/s_{u0s} = 0$; (b) $\mu = 0.5$, $m = 1$, $\sigma_s/s_{u0s} = 0$; (c) $\mu = 1$, $m = 1$, $\sigma_s/s_{u0s} = 0$; and (d) $\mu = 1$, $m = 1$, $\sigma_s/s_{u0s} = 2$

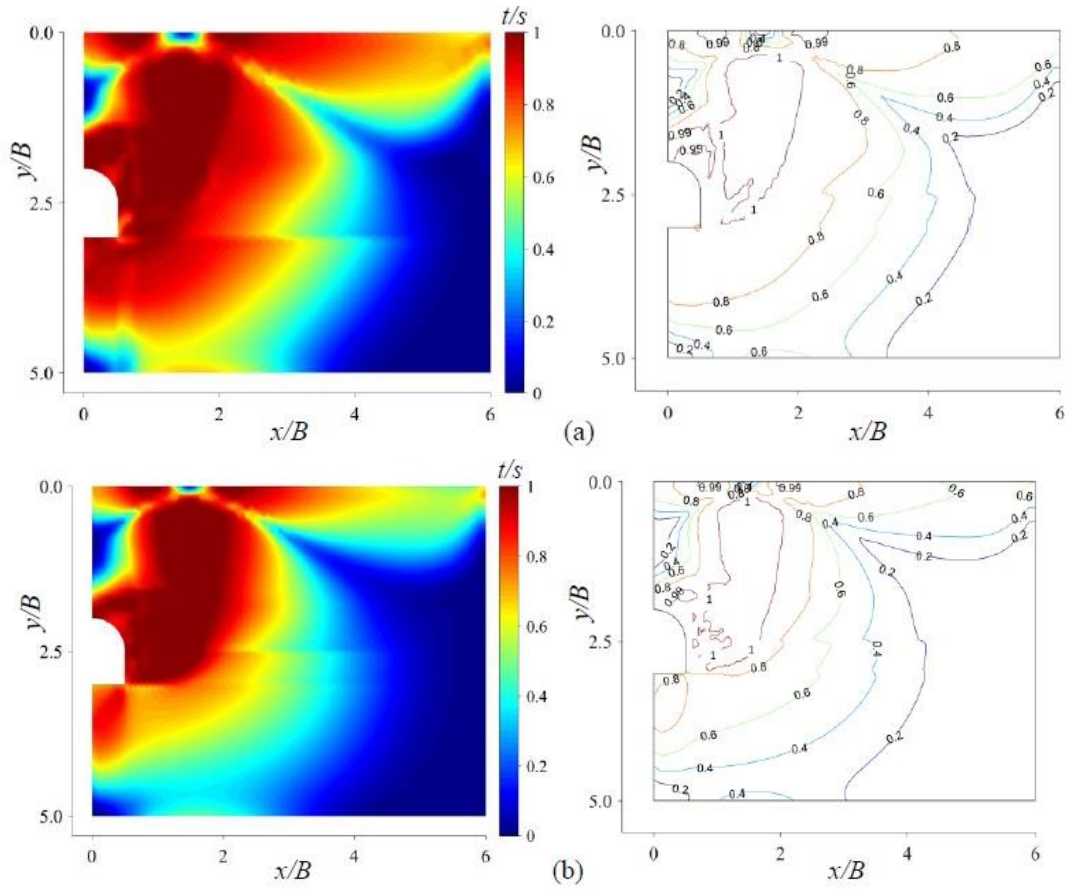

Fig. 11 Failure pattern and contour lines in HOC clay for C/B = 2, σ_s/s_{u0s} = 0, D/B = 1 and λ = 1.5: (a) μ = 0.5; and (b) μ = 1.25.

for μ smaller/higher than unity, respectively as illustrated in Table 2 and Fig. 8. It needs to mention that the height to width ratio (D/B) and anisotropic strength parameter (μ) have significant influence on the value of stability factor (N_s) as observed from Figs. 5-8 and Tables 1 and 2. The increase in the value of height to width ratio (D/B) reduces the stability of SASS tunnel, whereas the increase in the magnitude of μ enhances the stability of tunnel. For tunnel constructed in anisotropic NC/LOC clay, the value of stability factor continuously reduces with decrease in the value of rate of shear strength increment (m), which further goes on reducing with decrease in the value of C/B, as can be seen from Figs. 5-7 and Table 1.

6. Failure pattern

The zone of stress state at ultimate shear failure of surrounding soil mass around tunnel periphery i.e., shear failure at yielding has been generated for unlined SASS tunnels advanced in anisotropic NC/LOC and HOC clay taking into account the effect of σ_s, D, m and μ, as presented in Figs. 9-11. In order to visualize and interpret the zone of shear failure at yielding, a dimensionless factor (t/s) has been utilized.

Where

$$t = \left(\frac{\sigma_{yy} - \sigma_{xx}}{2} - \frac{s_{u0} - s_{u90}}{2} \right)^2 + \tau_{xy}^2 \left(\frac{s_{u0} s_{u90}}{s_{u45}^2} \right) \tag{11a}$$

$$s = \left(\frac{s_{u0} + s_{u90}}{2} \right)^2 \tag{11b}$$

The magnitude of t/s varies in between 0 to 1 i.e., the value of t/s equals to 1 represents the shear failure corresponding to stress state developed on Davis-Christian strength envelop; whereas, the value of t/s less than 1 signifies no shear failure corresponding to stress state generated inside the Davis-Christian strength envelop. Further, the magnitude of non-dimensional factor (t/s) has also been presented in the form of contour lines to provide an idea about the zone of shear failure, as illustrated in Figs. 9-11. It needs to be mentioned that the contour lines have been generated at an interval of 0.2 to avoid the cumbersome in the figures. It could be observed that the shape of the contour line corresponding to t/s =1 is matching with the shape of yielding zone (dark red color). For a given width of SASS tunnel, the size of shear failure at yielding continuously decreases with decrease in the height of the tunnel as can be seen from Fig. 9. The size of stress state at yielding is found to be (i) reducing with increase in the value of rate of shear strength increment (m)

as observed from the comparison between Figs. 10(a) and 10(b); (ii) greater for higher value of σ_s/s_{u0s} as seen by comparing Fig. 10(b) with Fig. 10(d); and (iii) smaller for higher value of μ as seen by comparing between parts (b) and (c) of Fig. 10 and parts (a) and (b) of Fig. 11.

It needs to be mentioned that the size of shear failure at yielding continuously increases with decrease in the degree of non-homogeneity and anisotropy of soil mass. This verifies the numerical results presented in Tables 1 and 2 and Figs. 5-8 that with decrease in the value of μ and m, the magnitudes of stability factor reduce.

7. Conclusions

In this paper, lower bound limit analysis in conjunction with finite elements and second order cone programming was applied for assessing the stability of unlined semi-circular arch with straight sides (SASS) tunnels in undrained clay. The non-homogeneity and anisotropy in undrained shear strength is considered in case of normally consolidated (NC) or lightly overconsolidated (LOC) clay, and heavily overconsolidated (HOC) clay is considered to be homogeneous anisotropic. The clay is assumed to follow Davis-Christian yield criterion. The influence of non-homogeneous parameter (m), anisotropic strength parameters (λ and μ) of soil, depth to width (D/B) and cover to width (C/B) ratio of the tunnel, and surcharge pressure (σ_s) on the ground surface on the stability factor (N_s) has been evaluated. Following are the specific conclusions that can be drawn from the current study:

- The value of stability factor (N_s) continuously increases with decrease in the value of surcharge pressure (σ_s/s_{u0s}) and depth to width (D/B) ratio of the tunnel; whereas it increases with increase in the value of cover to depth of tunnel for both NC/LOC and HOC clay. With increase in the value of C/B from 1 to 5, the magnitude of N_s for HOC undrained clay with λ = 1.5 and μ = 0.5 is observed to be increasing from (i) 1.20 to 3.46 with D/B = 0.5 and 1.11 to 2.57 with D/B = 1.5 for σ_s/s_{u0s} = 0; and (ii) (i) -0.59 to 1.55 with D/B = 0.5 and -0.63 to 0.82 with D/B = 1.5 for σ_s/s_{u0s} = 2.
- The magnitude of stability factor is the lowest for square section at lower part with semi-circular roof tunnel (D/B = 1.5) followed by tunnel having rectangular section at lower part with semi-circular roof (D/B = 1) and semi-circular arch tunnel (D/B = 0.5).
- With decrease in the value of m and μ, the magnitude of stability factor significantly reduces which indicates that anisotropy and non-homogeneity in terms of shear strength has considerably large influence on stability of tunnel. With decrease in the value of m from 1 to 0, the magnitude of N_s for NC/LOC undrained clay with D/B = 1; σ_s/s_{u0s} = 0 and C/B = 3 is observed to be reducing from (i) 8.43 to 2.35 for λ = 0.5 and μ = 0.5; and (ii) 11.81 to 3.37 for λ = 0.5 and μ = 1. The magnitude of stability factor is observed to be reducing for tunnels driven in anisotropic NC/LOC undrained clay in comparison to that constructed in isotropic undrained clay. Whereas, the stability factor for tunnel in HOC clay is higher or lower as compared to that in isotropic clay for μ greater or smaller than unity. For D/B = 1; σ_s/s_{u0s} = 0; m = 0 and C/B = 3, the magnitude of N_s is observed to be decreasing from 4.07 to 2.65 with undrained clay changes from isotropic (λ = 1 and μ = 1) to anisotropic NC/LOC (λ = 0.5 and μ = 0.5) clay. However, for D/B = 1; σ_s/s_{u0s} = 0; and C/B = 3, the magnitude of N_s is observed to be decreasing or increasing from 4.07 to 2.65 or 4.07 to 4.92 with undrained clay changes from isotropic (λ = 1 and μ = 1) to anisotropic HOC (λ = 1.5 and μ = 0.5) clay or anisotropic HOC (λ = 1.5 and μ = 1.5) clay, respectively.

References

Bishop, A.W. (1966), "The strength of soils as engineering materials", *Geotechnique*, **16**, 89-128. https://doi.org/10.1680/geot.1966.16.2.91.

Cao, X., Zhang, J. and Sun, D.A. (2022), "Drained cylindrical cavity expansion in K0-consolidated anisotropic soils under biaxial in-situ stresses", *Geomech. Eng.*, **28**(5), 493-503. https://doi.org/10.12989/gae.2022.28.5.493.

Casagrande, A. and Carillo, N. (1944), "Shear failure of anisotropic soils", *Contrib Soil Mech (BSCE)*, **1941-1953**, 122-135.

Chen, G.H., Zou, J.F. and Qian, Z.H. (2019), "An improved collapse analysis mechanism for the face stability of shield tunnel in layered soils", *Geomech. Eng.*, **17**(1), 97-107. https://doi.org/10.12989/gae.2019.17.1.097

Davis, E.H. and Christian, J.T. (1971), "Bearing capacity of anisotropic cohesive soil", *J. Soil Mech. Found. Divis. ASCE*, **97**(5), 753-769. https://doi.org/10.1061/JSFEAQ.0001594.

Davis, E.H., Gunn, M.J. Mair, R.J. and Seneviratine, H.N. (1980), "The stability of shallow tunnels and underground openings in cohesive material", *Geotechnique*, **30**(4), 397-416. https://doi.org/10.1680/geot.1980.30.4.397.

Drucker, D.C. (1953), "Limit analysis of two and three dimensional soil mechanics problems", *J. Mech. Phys. Solids*, **1**, 217–226. https://doi.org/10.1016/0022-5096(53)90001-5

Duncan, J.M. (1966), "Anisotropy and stress reorientation in clay", *J. Soil Mech. Found. Divis. ASCE*, **92**(4093 Proceeding).

Duncan, J.M. and Seed, H.B. (1966), "Anisotropy and stress reorientation in clay." *J. Soil Mech. Found. Divis. ASCE*, **92**(5), 21-50. https://doi.org/10.1061/JSFEAQ.0000909.

Du, D., Dias, D. and Yang, X. (2018), "Analysis of earth pressure for shallow square tunnels in anisotropic and non-homogeneous soils", *Comput. Geotech.*, **104**, 226-236. https://doi.org/10.1016/j.compgeo.2018.08.022.

Guo, Z., Liu, X. and Zhu, Z. (2021), "Limit analysis of seismic collapse for shallow tunnel in inhomogeneous ground", *Geomech. Eng.*, **24**(5), 491-503. https://doi.org/10.12989/gae.2021.24.5.491.

Hansen, J.B. and Gibson, R.E. (1949), "Undrained shear strengths of anisotropically consolidated clays", *Geotechnique*, **1**(3), 189-200. https://doi.org/10.1680/geot.1949.1.3.189.

Huang, M., Tang, Z., Zhou, W. and Yuan, J. (2018), "Upper bound solutions for face stability of circular tunnels in non-homogeneous and anisotropic clays", *Comput. Geotech.*, **98**, 189-196. https://doi.org/10.1016/j.compgeo.2018.02.015.

Hvorslev, M.J. (1960), "Physical components of shear strength of saturated clays", *Proceedings of the ASCE Research Conference on Shear Strength of Cohesive Soils*, Boulder, CO, 169-273.

Jakobson, B. (1955), "Isotropy of clays", *Geotechnique*, **5**, 23-28. https://doi.org/10.1680/geot.1955.5.1.23.

Khezri, N., Mohamad, H. and Fatahi, B. (2016), "Stability assessment of tunnel face in a layered soil using upper bound

theorem of limit analysis", *Geomech. Eng.*, **11**(4), 471-492. https://doi.org/10.12989/gae.2016.11.4.471.

Kumar, B. and Sahoo, J.P. (2020a), "Support pressure for circular tunnels in two layered undrained clay", *J. Rock Mech. Geotech. Eng.*, **12**(1), 135-148. https://doi.org/10.1016/j.jrmge.2019.04.007.

Kumar, B. and Sahoo, J.P. (2020b), "Support pressure for circular tunnels advanced below water bodies", *Tunn. Undergr. Sp. Tech.*, **97**, 103214. https://doi.org/10.1016/j.tust.2019.103214.

Kumar, B. and Sahoo, J.P. (2021), "Stability of unsupported circular tunnels in anisotropic normally and over consolidated saturated clay", *Comput. Geotech.*, **135**, 104148. https://doi.org/10.1016/j.compgeo.2021.104148.

Kumar, B. and Sahoo, J.P. (2023a), "Support pressure for stability of horseshoe-shaped tunnels in undrained clay using lower-bound finite-element limit analysis", *Int. J. Geomech.*, **23**(1), 04022264. https://doi.org/10.1061/(ASCE)GM.1943-5622.0002621.

Kumar, B. and Sahoo, J.P. (2023b), "Lining pressure for circular tunnels in two layered clay with anisotropic undrained shear strength", *Geomech. Geoeng.*, **18**(2), 91-104. https://doi.org/10.1080/17486025.2021.2012077.

Kumar, B. and Sahoo, J.P. (2023c), "Stability assessment of unlined real horseshoe-shaped tunnels in anisotropic and heterogeneous undrained clay", *Environ. Earth Sci.*, **82**(9), 1-16. https://doi.org/10.1007/s12665-023-10895-2.

Ladd, C.C. (1991), "Stability evaluations during stage construction", *J. Geotech. Eng.*, **117**(4), 540-615.

Lee, K.M. and Rowe, R.K. (1989), "Effects of undrained strength anisotropy on surface subsidences induced by the construction of shallow tunnels", *Can. Geotech. J.*, **26**(2), 279-291. https://doi.org/10.1139/t89-037.

Li, C. and Zoua, J.F. (2019), "Created cavity expansion solution in anisotropic and drained condition based on Cam-Clay model", *Geomech. Eng.*, **19**(2), 141-151. https://doi.org/10.12989/gae.2019.19.2.141.

Li, C., Zou, J.F. and Li, L. (2019), "Elasto-plastic solution for cavity expansion problem in anisotropic and drained soil mass", *Geomech. Eng.*, **19**(6), 513-522. https://doi.org/10.12989/gae.2019.19.6.513.

Lo, K.Y. (1965), "Stability of slopes in anisotropic soil", *J. Soil Mech. Found. Div.*, **31**, 85-106.

Lo, K.Y. and Milligan, V. (1967), "Shear strength properties of two stratified clays", *J. Soil Mech. Found. Div.*, **93**(1), 1-15. https://doi.org/10.1061/JSFEAQ.0000928.

Makrodimopoulos, A. and Martin, C.M. (2006), "Lower bound limit analysis of cohesive-frictional materials using second-order cone programming", *Int. J. Numer. Meth. Eng.*, **66**(4), 604-634. https://doi.org/10.1002/nme.1567.

MOSEK ApS, (2015), The MOSEK optimization toolbox for MATLAB manual. Copenhagen, Denmark: MOSEK ApS. Version 7.1 (Revision 28).

MATLAB [Computer software]. (2015), MathWorks, Natick, MA; 2015b.

Osman, A.S. (2010), "Stability of unlined twin tunnels in undrained clay", *Tunn. Undergr. Sp. Tech.*, **25**(3), 290-296. https://doi.org/10.1016/j.tust.2010.01.004.

Osman, A.S., Mair, R.J. and Bolton, M.D. (2006), "On the kinematics of 2D tunnel collapse in undrained clay", *Géotechnique*, **56**(9), 585-595. https://doi.org/10.1680/geot.2006.56.9.585.

Pan, Q. and Dias, D. (2016), "Face stability analysis for a shield-driven tunnel in anisotropic and nonhomogeneous soils by the kinematical approach", *Int. J. Geomech.*, **16**(3), 04015076. https://doi.org/10.1061/(ASCE)GM.1943-5622.0000569.

Rahaman, O. and Kumar, J. (2020), "Stability analysis of twin horse-shoe shaped tunnels in rock mass", *Tunn. Undergr. Sp. Tech.*, **98**, 103354. https://doi.org/10.1016/j.tust.2020.103354.

Saada, A.S. (1972). "Discussion on bearing capacity of anisotropic cohesive soil", *J. Soil Mech. Found. Div.*, **98**, 132-135.

Sahoo, J.P. and Kumar, B. (2019a), "Support pressure for stability of circular tunnels driven in granular soil under water table", *Comput. Geotech.*, **109**, 58-68. https://doi.org/10.1016/j.compgeo.2019.01.005.

Sahoo, J.P. and Kumar, B. (2019b), "Stability of circular tunnels in clay with an overlay of sand", *Int. J. Geomech.*, **19**(3), 06018039. https://doi.org/10.1061/(ASCE)GM.1943-5622.0001360.

Sahoo, J.P. and Kumar, B. (2021), "Peripheral stability of circular tunnels in anisotropic undrained clay", *Tunn. Undergr. Sp. Tech.*, **114**, 103898. https://doi.org/10.1016/j.tust.2021.103898.

Sahoo, J.P. and Kumar, J. (2012), "Seismic stability of a long unsupported circular tunnel", *Comput. Geotech.*, **44**, 109-115. https://doi.org/10.1016/j.compgeo.2012.03.015.

Sahoo, J.P. and Kumar, J. (2013a), "Stability of long unsupported twin circular tunnels in soils", *Tunn. Undergr. Sp. Tech.*, **38**, 326-335. https://doi.org/10.1016/j.tust.2013.07.005.

Sahoo, J.P. and Kumar, J. (2013b), "Stability of a long unsupported circular tunnel in clayey soil by using upper bound finite element limit analysis", *Proceedings of the Indian National Science, Academy*, **79**(64), 807-815. https://doi.org/10.16943/ptinsa/2013/v79i4/48005.

Sloan, S.W. (1988), "Lower bound limit analysis using finite elements and linear programming", *Int. J. Numer. Anal. Meth. Geomech.*, **12**(1), 61-77. https://doi.org/10.1002/nag.1610120105.

Sun, R., Yang, J., Liu, S. and Yang, F. (2021), "Undrained stability analysis of dual unlined horseshoe-shaped tunnels in non-homogeneous clays using lower bound limit analysis method", *Comput. Geotech.*, **133**, 104057. https://doi.org/10.1016/j.compgeo.2021.104057.

Ukritchon, B. and Keawsawasvong, S. (2018), "Lower bound limit analysis of an anisotropic undrained strength criterion using second-order cone programming", *Int. J. Numer. Anal. Meth. Geomech.*, **42**(8), 1016-1033. https://doi.org/10.1002/nag.2781.

Ukritchon, B. and Keawsawasvong, S. (2020), "Undrained stability of unlined square tunnels in clays with linearly increasing anisotropic shear strength", *Geotech. Geol. Eng.*, **38**(1), 897-915. https://doi.org/10.1007/s10706-019-01023-8.

Wilson, D.W., Abbo, A.J., Sloan, S.W. and Lyamin, A.V. (2014), "Undrained stability of dual square tunnels", *Int. J. Geomech.*, **14**(1), 69-79. https://doi.org/10.1061/(ASCE)GM.1943-5622.0000288.

Xu, J., Li, Y. and Yang, X. (2018), "Stability charts and reinforcement with piles in 3D nonhomogeneous and anisotropic soil slope", *Geomech. Eng.*, **14**(1), 71-81. https://doi.org/10.12989/gae.2018.14.1.071.

Yu, S. (2018), "Limit analysis of a shallow subway tunnel with staged construction", *Geomech. Eng.*, **15**(5), 1039-1046. https://doi.org/10.12989/gae.2018.15.5.1039.

Zhang, H., Chen, Q., Chen, J. and Wang, J. (2017). "Application of a modified structural clay model considering anisotropy to embankment behavior", *Geomech. Eng.*, **13**(1), 79-97. https://doi.org/10.12989/gae.2017.13.1.079.

Zhang, J., Feng, T., Yang, J., Yang, F. and Gao, Y. (2018), "Upper-bound stability analysis of dual unlined horseshoe-shaped tunnels subjected to gravity", *Comput. Geotech.*, **97**, 103-110. https://doi.org/10.1016/j.compgeo.2018.01.006.

CC